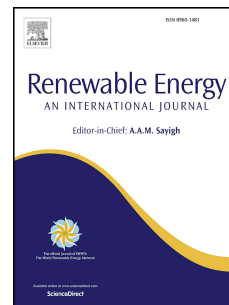


# Journal Pre-proof

Heterogeneous Acid Catalyst Preparation from Olive Pomace and its Use for Olive Pomace Oil Esterification

Manel AYADI, Sary AWAD, Audrey VILLOT, Manef ABDERRABBA, Mohand TAZEROUT



PII: S0960-1481(20)31772-9

DOI: <https://doi.org/10.1016/j.renene.2020.11.031>

Reference: RENE 14472

To appear in: *Renewable Energy*

Received Date: 21 October 2019

Revised Date: 21 September 2020

Accepted Date: 6 November 2020

Please cite this article as: AYADI M, AWAD S, VILLOT A, ABDERRABBA M, TAZEROUT M, Heterogeneous Acid Catalyst Preparation from Olive Pomace and its Use for Olive Pomace Oil Esterification, *Renewable Energy*, <https://doi.org/10.1016/j.renene.2020.11.031>.

This is a PDF file of an article that has undergone enhancements after acceptance, such as the addition of a cover page and metadata, and formatting for readability, but it is not yet the definitive version of record. This version will undergo additional copyediting, typesetting and review before it is published in its final form, but we are providing this version to give early visibility of the article. Please note that, during the production process, errors may be discovered which could affect the content, and all legal disclaimers that apply to the journal pertain.

© 2020 Elsevier Ltd. All rights reserved.

Credit Author Statement

Manel AYADI : Ph. D student: experiments design and realization, data acquisition and processing and writing paper

Sary AWAD: Supervisor, experiments design, paper writing.

Audrey VILLOT: Experiments design (activated carbon production), data processing and revision.

Manef ABDERRABBA: Supervisor, paper revision, getting student's funding.

Mohand TAZEROUT: Supervisor, paper revision.

Journal Pre-proof

## Heterogeneous Acid Catalyst Preparation from Olive Pomace and its Use for Olive Pomace Oil Esterification

Manel AYADI<sup>a,b</sup>, Sary AWAD<sup>a,\*</sup>, Audrey VILLOT<sup>a</sup>, Manef ABDERRABBA<sup>b</sup>, Mohand TAZEROUT<sup>a</sup>

a: department of Energy Systems and Environment (DSEE), IMT Atlantique

b: Laboratory of Materials, Molecules and Applications, University of Carthage, IPEST La Marsa Tunisia, Faculty of Sciences of Bizerte

**\* corresponding author :**

Sary AWAD, Energy Systems and Environment Department (DSEE), IMT Atlantique, 4 rue Alfred Kastler, 44307, Nantes, France.

**E-mail:** [sary.awad@gmail.com](mailto:sary.awad@gmail.com),

**Tel:** +33 2 51 85 85 61

# 1 Heterogeneous Acid Catalyst Preparation from Olive Pomace and its 2 Use for Olive Pomace Oil Esterification

3 Manel AYADI<sup>a,b</sup>, Sary AWAD<sup>a,\*</sup>, Audrey VILLOT<sup>a</sup>, Manef ABDERRABBA<sup>b</sup>, Mohand TAZEROUT<sup>a</sup>

4 a: department of Energy Systems and Environment (DSEE), IMT Atlantique

5 b: Laboratory of Materials, Molecules and Applications, University of Carthage, IPEST La Marsa Tunisia, Faculty  
6 of Sciences of Bizerte

7 \* **corresponding author** : Sary AWAD, Energy Systems and Environment Department (DSEE), IMT

8 Atlantique, 4 rue Alfred Kastler, 44307, Nantes, France. **E-mail:** [sary.awad@gmail.com](mailto:sary.awad@gmail.com), **Tel:** +33 2 51 85 85 61

## 9 **Abstract:**

10 Solid acid catalyst was produced from olive pomace (OP), characterized and used for the  
11 esterification of OP oil. OP was pyrolyzed, physical activated by steam and sulfonated using  
12 sulfuric acid. Commercial, coconut husk-based, activated carbon (CHAC) was also sulfonated  
13 for comparison. The activation has shown a significant increase in olive pomace activated  
14 carbon (OPAC) surface area by developing simultaneously its micro and meso-porosity. The  
15 sulfonation has further increased OPAC BET surface area to reach 618.18 m<sup>2</sup>/g and has  
16 changed its structure to become microporous. Sulfonation also removed tar residues and  
17 aliphatic hydrocarbons from OPAC's surface. Tendencies observed with carbon CHAC, used  
18 for comparison, are slightly different with a mesoporosity development. Although its higher  
19 surface area (1227.01 m<sup>2</sup>/g), CHAC has fixed three times less sulfur than OPAC, which can be  
20 attributed to its higher hydrophobicity or pore distribution. Sulfur was mainly fixed in the form  
21 of sulfonic acid (SO<sub>3</sub>H). Esterification with methanol using produced solid catalysts decreased  
22 OPO acidity below the 2 mg<sub>KOH</sub>/g threshold after 5 h of reaction and reduced mono, di and  
23 triglycerides to levels close to the ones required by European norm EN14214.

24 *Keywords:* Acid oil; biochar; esterification; olive pomace; solid acid catalyst;

25

Journal Pre-proof

26 *Nomenclature*

<i>Abbreviations</i>		<i>Variables</i>	
AC	Activated carbon	$C_s$	Molar fraction of specie $s$ (%)
AV	Acid value	$C_{N_2}$	Molar fraction of $N_2$ (%)
CHAC	Coconut Husk Activated Carbon	$k$	Irreversible reaction rate constant ( $h^{-1}$ )
CHACS	Sulfonated Coconut Husk Activated Carbon	$k_1$	Direct reaction rate constant ( $h^{-1}$ )
FFA	Free Fatty Acids	$k_2$	reverse reaction rate constant ( $h^{-1}$ )
OP	Olive Pomace	$M$	Methanol concentration ( $mol.l^{-1}$ )
OPAC	Olive Pomace Activated Carbon	ME	Methyl ester concentration ( $mol.l^{-1}$ )
OPACS	Sulfonated Olive Pomace Activated Carbon	$m_s$	Mass of specie $s$ (g)
OPO	Olive Pomace Oil	$M_s$	Molar mass of specie $s$ ( $g.mol^{-1}$ )
TOF	Turn Over Frequency	$Q_{N_2}$	Nitrogen flowrate (l/min)
TOF <sub>1h</sub>	Turn Over Frequency after 1 h of reaction	$V_s$	Molar volume of specie $s$ ( $l.mol^{-1}$ )
TOF <sub>5h</sub>	Turn Over Frequency after 5 h of reaction	$W$	Water concentration ( $mol.l^{-1}$ )

27

28

## 29 **1- Introduction:**

30 Tunisia is ranked second in the world in the production of olive oil with a number of trees  
31 exceeding 86 million. Oil represents only 20% of olives mass, the remaining fraction exits oil  
32 production process in forms of solid and liquid wastes (30% and 50% respectively) [1].

33 Olive pomace (OP), the solid by-product of olive oil, contains pieces of pit (42–54%), about  
34 10–11% skin, and between 21 and 33% of pulp [2] and has an oil content that could reach 8%  
35 depending on extraction technology [2].

36 OP has a negative impact on the environment due to slightly acidic pH values, a high moisture  
37 content and a very high content of organic matter (lignin, hemicellulose and cellulose). Olive  
38 pomace is non-biodegradable due to its significant contents of water-soluble phenolic  
39 substances. Besides that, olive pomace contains water-soluble fats, proteins, water-soluble  
40 carbohydrates and it is rich in potassium and poor in phosphorus and micronutrients [3]. Olive  
41 pomace composition attributes it phytotoxic and antimicrobial properties [4]. Since OP is still  
42 rich in oil and polyphenol, it increases soil hydrophobicity and infiltration rate and decreases  
43 water retention rate in case of land spreading [5]. These environmental problems could be  
44 eliminated if the olive residue is either treated to extract olive pomace oil residue or used to  
45 obtain fuel [6]. However, this step increases process costs, and resolves partially the problem,  
46 because exhausted OP and extracted oil are still wastes that need to be treated. However, the  
47 valorization of these wastes into biosourced-materials and/or energy carriers, could enhance the  
48 economy of the process. For example, exhausted olive pomace can be used to produce activated  
49 carbon, while olive pomace oil (OPO) can be used for biodiesel production. However, OPO has  
50 a very high content of free fatty acids (FFA) which requires the use of acid catalysis followed  
51 by alkali catalysis. Among different types of catalysts, heterogeneous ones are preferable

52 because of their lower corrosiveness, their reusability and for the ease of separation during  
53 process.

54 Several studies have been led on the use of sulfonated char and activated carbon as solid  
55 catalysts for esterification of FFA because of sustainability and integrability in processes. In  
56 fact, these materials are byproducts of biorefineries and their use reduces the need for metal  
57 catalysts and fossil fuel derived ones [7]. Furthermore, these catalysts present the advantage of  
58 having very high specific surface area ranging from 200 to 1500 m<sup>2</sup>/g besides their non-polarity  
59 that prevents them from being deactivated because of water and/or glycerol produced during  
60 esterification and/or transesterification reactions [8]. In fact, hydrophilic structures, adsorbs  
61 water generated during esterification reaction which deactivates acid sites [9].

62 Carbon based catalysts can be obtained by simply impregnating char/activated carbon with  
63 sulfuric acid [10] or by exposing it to SO<sub>3</sub> [8] in order to functionalize the surface with sulfonic  
64 acid (SO<sub>3</sub>H).

65 Extensive research on sulfonated AC conducted by Dekhoda et al [11] prove that the more  
66 powerful the use of the sulfonating agent, the higher the acid density in the catalysts is  
67 produced. These results are in agreement with the results of Kastner et al. who made a  
68 comparative study between sulfonated AC prepared from biochar and wood-based materials.  
69 They examined the catalytic activity of catalysts during the esterification of fatty acids.  
70 According to their work the sulfonated AC catalyst made from wood is more efficient because  
71 of its higher activity. However, catalyst reuse was not possible due to water absorption and -  
72 SO<sub>3</sub>H leaching, which leads to a decrease in its specific surface area and a reduction in acid  
73 density similar to other sulfonated AC [8].

74 The aim of the present work is to investigate the production of a solid acid catalyst from olive  
75 pomace by pyrolysis/activation followed by a sulfonation using sulfuric acid. To the knowledge

76 of the authors this cheap and highly available raw material is not well explored in literature.  
77 There are few works that dealt with the production and characterization of biochar and on its  
78 use as an adsorbent [3]. No works were found in literature about AC production from olive  
79 pomace neither on its use as a catalyst for esterification. The originality of the present work  
80 resides in the suggestion of an integrated solution for the production of AC and biodiesel from  
81 olive oil by-products. The produced solid catalyst can compete at the same time with  
82 homogeneous catalysts and with Commercial, coconut husk activated carbon -based solid  
83 catalyst.

## 84 **2- Materials and methods**

### 85 *2.1. Raw materials and chemicals*

86 Olive pomace and olive pomace oil used in this study were supplied by Abou El-Walid  
87 Company located in Tunisia. In this company, hexane extraction is used to recover pomace oil.  
88 This oil has a high content of FFA reaching 60 wt.%. The remaining are mono, di and  
89 triglycerides (glycerides) and it has a kinematic viscosity of 26.8 mm<sup>2</sup>/s at 40°C. FFA are  
90 mainly composed of oleic Acid (57%), palmitic acid (16.5%), linoleic acid (15.7%) and stearic  
91 acid (4%). Its mean molecular weight is 292 g/mol.

92 Commercial, coconut husk based activated carbon, (CHAC) used in this work for comparison  
93 was furnished by Jacobi Carbons France (PICA).

94 Methanol having 98% purity and 17 M sulfuric acid were purchased from Sigma-Aldrich

### 95 *2.2. Olive Pomace and Olive Pomace Oil characterization*

#### 96 *2.2.1 Chemical analysis:*

97 Olive pomace was dried and grinded (by RETSCH MM400 scale series laboratory mill) and  
98 sieved to powder of sizes < 1 mm. The organic composition of raw materials, CHNS and O,  
99 was measured by A Thermofinnigan EA 1112 elemental analyzer (Thermo-finnigane  
100 instrument). Same procedure was also applied for biochar, activated carbons and catalysts  
101 elemental analysis. The inorganic composition of raw materials was analyzed by X-ray  
102 fluorescence spectrometry (SHIMADZU EDX-500HS) which is a semi-quantitative method.  
103 The error percentage of this analysis is considered to be around 20% for the main elements in  
104 ash composition.

### 105 2.2.2. TGA analysis

106 The proximate analysis was carried out using a SETSYS Evolution Thermogravimetric  
107 Analyzer (TGA) following the ASTM standards: ASTM D3175 [12] for volatile matter. TGA  
108 was also used to determine the lignocellulosic material content distribution, for that the olive  
109 pomace materials were heated under an inert gas flow to a final temperature of 900 °C with a  
110 heating rate of 10 °C.min<sup>-1</sup>, with intermediate plateaus at 100°C, 250 °C, 350 °C and 500 °C  
111 corresponding to the evaporation of moisture and the final degradation temperatures of  
112 hemicellulose, cellulose and lignin respectively [13].

113 To conduct the analysis, protective gas, argon, is passed through the thermobalance to protect it  
114 from possible corrosive gases. The process was carried out on samples weighing between 3 mg  
115 – 10 mg. a flow of nitrogen of 100 cm<sup>3</sup>.min<sup>-1</sup> was used to ensure an inert condition and the  
116 removal of the pyrolytic gases.

### 117 2.2.3. Ash content of olive pomace and carbonaceous supports

118 The ash content of different products was determined by placing dry samples in a laboratory  
119 muffle furnace (Nabertherm p330) Following the ASTM D1102 [14] for ash content of the  
120 biomass and ASTM D3174 [15] for ash content of the char.

121 2.2.4. Determination of olive pomace oil (and methyl esters) acid value:

122 The acid value is determined by titration of the oil (before and after esterification) using a  
 123 standardized titration solution of KOH in ethanol, according to the ASTM D664 method [16].

### 124 **2.3. Preparation of heterogeneous catalyst**

#### 125 *2.3.1. Preparation of pyrolysis char and activated carbon*

126 Olive pomace is pyrolyzed up to 800°C with a heating rate of 10°C/min under nitrogen flow  
 127 using setup presented in fig 1. For that, 400 g of olive pomace were introduced in a semi-  
 128 rotating quartz tube under N<sub>2</sub> flow of 0.75 SLPM (standard liters per minute measured at 100  
 129 kPa and 0°C). At the end of this step, it is possible to cool-down the system at room  
 130 temperature. The raw char, denoted hereafter as Biochar, and the condensable phase can be  
 131 collected and weighted. The condensable gases (steam and light tars) were removed by a cold  
 132 trap close to 0 °C and the gases analyzed by the GC. The pyrolysis gas was analyzed by online  
 133 gas micro-chromatography (SRA Instruments R 3000) equipped with a thermal conductivity  
 134 detector. This technique was able to measure the non-condensable gases such as H<sub>2</sub>, O<sub>2</sub>, N<sub>2</sub>,  
 135 CH<sub>4</sub>, CO, CO<sub>2</sub>, C<sub>2</sub>H<sub>4</sub>, C<sub>2</sub>H<sub>6</sub>, C<sub>3</sub>H<sub>8</sub> and C<sub>3</sub>H<sub>6</sub>. The system performed a complete analysis every 3  
 136 min, and the mass of each gaseous specie ( $m_s$ ) was evaluated by the expression given in  
 137 equation 1 [19]:

$$138 \quad m_s = M_s \frac{Q_{N_2}}{V_m} \int_{t_0}^{t_f} \frac{C_s}{C_{N_2}} dt \quad (1)$$

139 where the interval of integration corresponds to the elapsing time of analysis,  $C_s$  represents the  
 140 molar fraction of the detected species and  $M_s$  its molecular weight,  $Q_{N_2}$  is the nitrogen flow rate  
 141 and  $C_{N_2}$  the nitrogen molar fraction, and  $V_m$  is the molar volume. The pyrolysis was repeated at  
 142 least 3 times and the average biochar yield was close to  $30.8 \pm 0.3\%$ .

143 In order to produce activated carbon, superheated steam was used in order to increase the  
144 specific surface area of the biochar and increase its microporosity. When the temperature of  
145 800°C is reached, the nitrogen atmosphere is switched to a nitrogen/steam mixture (0.53 SLPM  
146 / 88 vol. % of N<sub>2</sub> and 0.7 mL.min<sup>-1</sup> of H<sub>2</sub>O / 12 vol. %). The activated chars were denoted as  
147 OPAC.

### 148 *2.3.2. Sulfonation of biochar and activated carbon:*

149 Biochar, OPAC and CHAC are sulfonated using 17 M Sulfuric acid, under vigorous stirring  
150 during 15 min. Excess acid was eliminated by decantation and solid residue was poured into a  
151 ceramic crucible and introduced to muffle furnace preheated to 100°C and kept during 18 h.  
152 Finally, sulfonated material was profusely washed with distilled water before being dried in  
153 oven at 105°C overnight. Washing step was performed in order to ensure that the remaining  
154 SO<sub>3</sub>H sites are highly stable. Washing consisted on several soaking and pouring, through a  
155 sieve, steps with distilled water until the water leaving sieve is neutral. Then catalyst was  
156 soaked in water, stirred for 2 h, then left overnight before pouring water and verifying its pH  
157 stability.

158 As per sulfuric acid/OP ratio. The ratio was optimized by impregnating different amounts of  
159 sulfuric acid on OPAC and by realizing an acid esterification for 1 h of OP. Optimization  
160 started by using the amount suggested by Kastner et al. [8] and it was each time divided by 2  
161 until noticing a significant decrease in catalytic activity. The optimal amount that was found is  
162 0.4 g<sub>H<sub>2</sub>SO<sub>4</sub></sub>/g<sub>AC</sub> and it was adopted for the sulfonation of different carbonaceous materials used  
163 in this study.

## 164 *2.4 Biochar, Activated carbon and Catalyst analysis:*

### 165 *2.4.1 BET surface and porosity analysis*

166 The specific surface area was determined using the Brunauer-Emmet-Tellet (BET) method  
167 under nitrogen adsorption/desorption isotherms of nitrogen at - 196 °C (Micromeritics ASAP  
168 2020). This model is based on the principle of formation of multilayers but only the first layer  
169 of adsorbate molecules is attached to the solid surface by adsorbent-adsorbate adsorption  
170 forces. Currently BET model is the most applied to determine surface areas thus it can be taken  
171 as a reference method [20]. The Barrett-Joyner Halenda (BJH) and Horvath Kawazoe methods  
172 were respectively used to characterize the microporosity (pore diameters < 2 nm) and the  
173 mesoporosity (2 < pore diameters < 50 nm) [21].

#### 174 2.4.2. X-ray diffraction analysis (XRD):

175 XRD is usually used to determine the patterns existing in the structure of materials. Typically,  
176 it determines the crystallinity degree of a material and the type of crystalline structure.  
177 Furthermore, due to a large library of spectra it is also possible to determine the nature of stacks  
178 or clusters present in the material (aromatic, aliphatic, unsaturated ...).

179 The XRD patterns were monitored by X ray diffraction ex-situ using the apparatus Siemens D-  
180 5000. It is focused by a Ge crystal primary monochromator of which Ni-filtered Cu K $\alpha$ 1  
181 radiation,  $\lambda = 1.54056 \text{ \AA}$ , with  $\theta/ 2\theta$  diffraction instrument operating in reflection  
182 geometry, and the tube of copper is run at 40 mA and 40 kV.

#### 183 2.4.3. Fourier Transform Infrared Spectroscopy analysis (FT-IR):

184 FTIR spectroscopy was carried out in an ATR Bruker Tensor 27, model 2012. Spectra were  
185 recorded in the range 4000-400  $\text{cm}^{-1}$ , 50 scans were taken at a 0.1  $\text{cm s}^{-1}$  scan rate and 2  $\text{cm}^{-1}$   
186 resolution. This technique is used to determine the chemical functions and bonds present on the  
187 surface of analyzed materials. In this study it helps to determine the chemical bonds in which  
188 sulfur, that was fixed on the material, is involved. Furthermore, it could help to detect the

189 presence of other species present on the surface of activated carbon that could also play a role  
190 in the catalysis of esterification reaction.

#### 191 *2.4.4 Scanning Electron Microscopy (SEM):*

192 A scanning electron microscope SEM, **JEOL JSM 7600F**, **JEOL JSM 5800LV** equipped with  
193 a SDD SAMx energy dispersion spectrometer and JEOL (hybrid of two microscopes), was used  
194 to characterize the surface morphologies of carbonaceous materials.

#### 195 *2.4.5. X-Ray Fluorescence spectrometry (XRF):*

196 Bulk chemical composition of different materials was determined with a "SHIMADZU" X-ray  
197 fluorescence (XRF) analyzer fitted with an EDX 800 HS X-ray tube, a gas scintillation detector  
198 and a PR-10 anode. Analyzed materials were dried, crushed and sieved before analysis. 0.5 g  
199 samples were used each time. CHON analysis results were taken in consideration during XRF  
200 results treatment.

#### 201 *2.4.6. Micro-GC*

202 Gas chromatography is used to determine the molar (or volume) composition of gases produced  
203 during pyrolysis and activation processes. The apparatus used is a G2801A Model 3000A  
204 Micro GC gas chromatography (Agilent Technologies, China), having two independent  
205 systems (A and B) each consisting of an injector, a column and a thermal conductivity detector  
206 (TCD). Both systems use Argon as the carrier gas.

207 The detector of system A makes it possible to identify H<sub>2</sub>, CH<sub>4</sub>, CO and N<sub>2</sub>. The system B  
208 detector identifies CO<sub>2</sub>, H<sub>2</sub>O, C<sub>2</sub>H<sub>2</sub>, C<sub>2</sub>H<sub>4</sub>, C<sub>2</sub>H<sub>6</sub>, C<sub>3</sub>H<sub>6</sub>, C<sub>3</sub>H<sub>8</sub>, C<sub>4</sub>H<sub>6</sub>, C<sub>4</sub>H<sub>8</sub> and C<sub>4</sub>H<sub>10</sub>.

#### 209 *2.4.7. Hydrophobicity*

210 After drying the OPAC and CHAC samples, they are placed in a stainless steel support with a  
 211 mesh size of 0.8 mm. These samples are swept by a dry air flow of 50 cm<sup>3</sup>/min and by a stream  
 212 of water vapor whose humidity is 50%. The measurement of the hydrophobicity was made at  
 213 ambient temperature and atmospheric pressure. The parameters of the "dry airflow and water  
 214 vapor flow" experiment are set using a humid air generator, "OMICRON Technologies",  
 215 introduced into a reactor at a total flow of 15 cm<sup>3</sup>/min, during 3 h. At the end of the  
 216 humidification, OPAC and CHAC are weighed and put in the oven at 105 °C for 18h, and then  
 217 they are reweighed to calculate the amount of absorbed moisture.

### 218 ***2.5. Pyrolysis and activation's gaseous products analysis***

219 At the outlet of reactor, gas samples were collected and injected into a micro-GC for analyzer.  
 220 Samples were taken during pyrolysis and activation at time intervals of 10 min in order to  
 221 detect the following gases: H<sub>2</sub>, CO, CO<sub>2</sub>, CH<sub>4</sub> and light hydrocarbons (C<sub>x</sub>H<sub>y</sub>). An additional  
 222 sample was taken 2 min after steam injection in order to highlight the shift between pyrolysis  
 223 and activation. The molar composition of gases was set after subtracting the N<sub>2</sub> fraction.

### 224 ***2.6. Olive Pomace Oil Esterification***

225 Olive pomace oil esterification was performed in a batch reactor at 60°C under vigorous  
 226 stirring during 5 h. Heterogeneous catalysis was performed using different methanol to FFA  
 227 molar ratios (3:1, 6:1 and 9:1) and different loads (10, 15 and 20 wt.%) of produced  
 228 heterogeneous catalyst. Homogeneous catalysis was performed, for comparison, using 3.6 wt%  
 229 of 17 M sulfuric acid and 3:1 methanol to FFA ratio. Turn Over Frequency (TOF) was  
 230 calculated for homogeneous and heterogeneous catalysts under different conditions for  
 231 comparison. TOF was calculated as follows (eq 2).

$$232 \quad TOF(h^{-1}) = \frac{FFA_0 - FFA_t}{SO_3H.t} \quad (2)$$

233 Where  $FFA_0$  and  $FFA_t$  (moles) are the amounts of free fatty acids at the beginning and at time  $t$   
234 of reaction.  $SO_3H$  (moles) is the number of moles of acid sites present in catalyst calculated  
235 based on the elemental analysis of heterogeneous catalyst. For homogeneous catalyst the  
236 number of moles of  $H^+$  was used.

237 Reaction order and rate constant ( $k$ ) were determined for different studied reactions using the  
238 integral method in order to understand underpinned phenomena observed for different  
239 conditions.

#### 240 2.7. GC-FID/MS Analysis

241 Gas chromatography coupled to flame ionization detector and to mass spectrometer (GC-  
242 FID/MS) was used in order to determine the contents of fatty acid methyl esters, mono, di, and  
243 triglycerides in oil samples and on the products having the lowest acid values using ASTM  
244 method D 6584 [16]. This analysis will shed lights on the effects of used catalyst on  
245 transesterification also.

246 The used GC column is an open tubular one with 5% phenylpolydimethylsiloxane bonded and  
247 cross linked phase internal coating. FID temperature was set to 380°C. The column, is 15 m  
248 long, has an internal diameter of 0.32 mm and 0.1  $\mu\text{m}$  film thickness. 3 mL/min of hydrogen  
249 was used as carrier. Internal standards used are butantriol and tricaprane that were injected in  
250 ratios 1:1:1 with respect to analyzed sample. Derivatization was ensured using N-methyl-N-  
251 trimethylsilyltrifluoroacetamide (MSTFA). The mass spectrometer was set at an ionizing voltage  
252 of 70 eV and a range of  $m/z$  30–450 respectively.

#### 253 2.8. Viscosity measurement

254 Viscosity is a good indicator on the conversion rate of glycerides [17] as the viscosity of methyl  
255 esters is between 6 – 12 times lower than that of triglycerides [18]. Thus, it was applied on the

256 samples having the lowest acid value (AV) in order to compare them to raw oil and to check  
 257 out the effects of catalyst on transesterification.

258 Dynamic viscosity was measured at 40°C using an AND vibro viscometer. Density was  
 259 measured using a pycnometer M50T (850 – 900 g/l) with a precision of 1 g/l. then kinematic  
 260 viscosity was obtained by dividing it by the density according to test method EN ISO 3104  
 261 [19].

### 262 **3- Results and discussion:**

#### 263 **3.1. Pyrolysis and activation of olive pomace**

264 In order to understand the impact of the pyrolysis and activation processes on the solid phase,  
 265 gaseous products composition (CO<sub>2</sub>, CO, CH<sub>4</sub>, H<sub>2</sub> and light hydrocarbons (C<sub>x</sub>H<sub>y</sub>) ) was  
 266 followed all along the processes. At the first stage of reaction, CO and CO<sub>2</sub> started to appear at  
 267 230°C reaching a peak production between 350 and 370 °C which can be attributed to  
 268 dehydration and decarboxylation of cellulose and hemicellulose [22]. CH<sub>4</sub> peak occurring  
 269 between 560 and 620°C indicates lignin degradation. With temperature increasing from 480 to  
 270 800 °C the production of H<sub>2</sub> started and increased significantly as temperature increased. H<sub>2</sub> is  
 271 a result of severe cracking of intermediary products and char that continues to emit light  
 272 volatiles at high temperature levels [23]. Degradation ends at 580°C, temperature at which CO,  
 273 hydrocarbons and CH<sub>4</sub> start decaying. At 680°C severe cracking of char continues to emit light  
 274 volatiles (tar present in its pores and on its surface) at high temperature levels. These reactions  
 275 are accompanied by a drastic increase in H<sub>2</sub> and C<sub>x</sub>H<sub>y</sub> production following dehydrogenation  
 276 (eq. 3) and carbonization (eq. 4) reactions. CO also increases due to these reactions added to  
 277 the decomposition of CO<sub>2</sub> into CO at high temperatures [24].





280 During pyrolysis, the heteroatoms are removed as volatiles. These degradation reactions  
 281 introduce a rearrangement of the carbon atoms, which form stacks of polyaromatic graphite  
 282 layers. Graphite is a layered structure in which the graphene layers are formed by carbon atoms  
 283 bonded by  $\sigma$  and  $\pi$  bonds to three other neighboring carbon atoms.

284 At 800 °C ( $t = 80$  min) superheated water steam is injected during 80 min which corresponds to  
 285 the activation step. As it can be noticed in fig 2, 2 min right after the beginning of steam  
 286 injection, methane has drastically decreased while sharp increases of hydrogen, carbon dioxide  
 287 and hydrocarbons have been noticed. These results are in accordance with reactions 5 and 6,  
 288 where the activation step releases  $H_2$ . Hydrogen started to decrease right after the peak and  
 289 started to stabilize after 20 min at 55%. Methane production also continues decreasing until  
 290 reaching a plateau of 1.7% after 30 min



293 CO volume concentration slightly increases from 17% to 21% during the first 30 min after  
 294 steam injection before starting a linear decrease reaching 14% at steam cut-off. Carbon dioxide  
 295 increases drastically from 0% (2 min after steam injection) up to 28% at steam cut-off.

296 The trends of these curves reveals the following reactional scheme:

297 Right after steam injection dehydrogenation and carbonization reactions continue to occur and  
 298 water steam triggers water-gas reaction that involves solid carbon (eq 5) and steam methane  
 299 reforming (eq 7). That explains the sharpening of  $H_2$  and  $CH_4$  slopes



301 After 2 min of reaction, the available amount of tar present in the pores and on the surface of  
302 char starts to decrease, which leads to lower rates of reactions 3, 5 and 7 and to the decrease of  
303 curves slopes. At this stage, H<sub>2</sub> starts to decrease and CH<sub>4</sub> slope becomes less steep. At this  
304 moment water gas shift reaction (eq 6) is triggered where produced CO starts to oxidize into  
305 CO<sub>2</sub>. This reaction is triggered due to the lack of methane that has a more affinity to water  
306 steam at these temperatures. After 30 min, when methane reforming decays, the trade-off  
307 between CO and CO<sub>2</sub> can be clearly noticed.

308 Among the up-listed reactions, water-gas and carbonization reactions affect the structure of  
309 activated carbon. The atmosphere of the oven containing H<sub>2</sub>O makes it possible to develop  
310 cone-shaped pores, generated by carbon gasification reactions Eq.6. These observations are  
311 consistent with the results reported by Prauchner M. and Rodriguez-Reinoso F. [25] for  
312 activated carbon produced from coconut shells.

### 313 *3.2 Characterization of olive pomace, biochar, activated carbon and catalysts*

#### 314 *3.2.1 Proximate and ultimate analysis:*

315 The elemental compositions of olive pomace and carbonaceous materials are given in Table 1.  
316 Olive pomace has a high oxygen content reaching 41.51% of its weight. It contains 22.77%  
317 Cellulose, 19.8% Hemicellulose, 17.8% lignin, 21% fixed carbon and 0.32% Ash. The analysis  
318 results are comparable to those found elsewhere in literature [26]. Fixed carbon content of olive  
319 pomace makes it a good raw material for the preparation of activated carbon, because, it  
320 reflects the total carbon present in the final product [27].

321 After pyrolysis, oxygen content of bio-char has been reduced to 4.4 % due to decarboxylation  
322 and dehydration reactions. Hydrogen content was also reduced to 1.76% due to dehydration  
323 and depolymerization reactions. This evolution is explained by the breaking of the weakest  
324 chemical bonds (C-O, C-H) under the temperature effect [26]. According to the literature, the

325 increase of pyrolysis temperature increased the elimination of heteroatoms (O, H, N) in the  
326 form of volatile compounds is accentuated as well as the carbon content and the aromaticity of  
327 the char [29]. Nitrogen and oxygen that remain inside the char could be possibly embedded  
328 inside the biomass far from the surface. In fact, nitrogen and oxygen that leave out in form of  
329 volatile matter are most likely on the surface of feedstock where they can react with light free  
330 radicals before being swept out of the reactor. Nitrogen and oxygen inside the organic matter  
331 have more chances to recombine with carbon atoms and to integrate the solid carbon matrix.  
332 The pyrolysis allowed to limit the mineral species volatilization (an increase of ash rate),  
333 resulting in a highly concentrated carbon and mineral species in the matrix of the char.

334 Activation has further concentrated carbon by decreasing the content of all other components.  
335 Carbon content passed from 77.95% to 85% and oxygen, nitrogen and hydrogen have been  
336 decreased by half. Ash content has also slightly increased due to this step. OPAC has similar  
337 elemental composition to CHAC. Differences lie mainly in a lower carbon content of OPAC  
338 and a slightly higher ash and nitrogen contents.

339 The sulfonation of bio-char has not apparently succeeded. Sulfur content was lower than  
340 CHONS analyzer detection limits after sulfuric acid treatment. While carbon and hydrogen  
341 contents have decreased, nitrogen and oxygen contents have increased. A slight increase of ash  
342 content has been also detected. These observations indicate that sulfuric acid has mainly  
343 attacked the surface of bio-char and did not get deeper inside the material.

344 Sulfonation of OPAC and CHAC led to sulfur fixation that was accompanied by carbon  
345 contents decrease and oxygen increase by almost 5 folds for OPAC and 3 folds for CHAC. It  
346 was observed also that oxygen increase was proportional to sulfur fixation which could be  
347 explained by the fixation of  $-\text{SO}_3\text{H}$  functional group on the surface of the catalyst [30].

348 *3.2.2 BET analysis*

349 The analysis of adsorption and desorption isotherms is done in order to get information about  
350 porous structure of activated carbon OPAC, CHAC, OPACS and CHACS. According to  
351 IUPAC classification, the N<sub>2</sub> adsorption-desorption isotherms of CHAC and CHACS, deemed  
352 to be type I, thus confirming the typical characteristics of porous activated carbon. OPAC and  
353 OPACS considered, deemed to be type IV, is typical for many ordered organic-inorganic  
354 nanocomposites with accessible mesopores although when the size of these pores is close to the  
355 micropore range or pore size distribution is broad, type I isotherms can be observed. This is  
356 also supported by the volume distribution between micro and mesoporous volume given in the  
357 Table 2 with a ratio of micropore of 44 and 62 % for OPAC and OPACS respectively.

358 Results of BET are shown in Table 2. As expected, the external surface, the pore size and the  
359 microporous volume are clearly favored after steam physical activation. We can conclude that  
360 steam activation produces activated carbons with a pronounced development of microporosity  
361 at the expense of mesoporosity as stated in other research works found in the literature [31].

362 The BET surface area of OPAC and CHAC were respectively 345 and 1227 m<sup>2</sup>g<sup>-1</sup> and the total  
363 pore volume and micropore volume were 0.240 cm<sup>3</sup>g<sup>-1</sup> and 0.106 cm<sup>3</sup>g<sup>-1</sup> (44 % of total  
364 volume), respectively, for OPAC and 0.542 cm<sup>3</sup>g<sup>-1</sup>. and 0.380 cm<sup>3</sup>g<sup>-1</sup> (70.1 % of total volume)  
365 for CHAC. The treatment with sulfuric acid has a significant impact on the porous structure,  
366 notably by increasing the specific surface area of 44 and 12.4 % for OPACS and CHACS  
367 respectively. These observed phenomena could be due to impurities found in activated carbon  
368 before sulfonation and which can block some of the pores [32], the sulfuric acid will play the  
369 role of a cleaner that eliminates the impurities and opens pores clogged by tar.

370 Nevertheless, the volume of micropores of CHAC decreased after treatment with H<sub>2</sub>SO<sub>4</sub> to  
371 create other mesoporous volumes. Increasing the surface and creating a mesoporous volume  
372 can be attributed to the generation of gases from the reaction between the acid and the materials  
373 on the surface of the carbon, which reopens the closed micropores and creates new mesopores

374 [33]. However, micropores volume has increased with OPAC at the expense of mesopores. For  
375 instance, micropores occupied 44 % of total porosity, after sulfonation, OPACS micropores  
376 represent 61.8 % of total pores volume, while it decreased from 70.1 % with CHAC to 35%  
377 with CHACS.

378 Although its higher specific surface, CHAC has a lower fixation rate of sulfur, this is probably  
379 due to the hydrophobicity of their surface that reduces surface wetting necessary for  
380 impregnation. Indeed, several studies have demonstrated that the polar sites of all activated  
381 carbon attract water molecules, with different percentages depending on the raw material and  
382 the process of manufacturing activated carbon, which enhances the adsorption of hydrophilic  
383 compounds in the micropores [34].

384 Another reason could be a disparity in ionic exchange capacity between OPAC and CHAC  
385 which allows the former to fix more sulfonic acid on its surface [35].

### 386 3.2.3. X-ray diffraction analysis (XRD):

387 The XRD pattern for the activated carbon and sulfonated activated carbon are illustrated in  
388 Fig 3. The diffractogram recorded that all carbonaceous materials have shown two peaks  
389 located at  $2\theta = 22.5^\circ$  and  $44^\circ$ , respectively, corresponding to the diffraction by graphite planes  
390 of index (002) and (100), respectively.

391 The results show that the broad diffraction peak ( $2\theta = 10-25^\circ$ ) can be attributed to the  
392 amorphous structure as a major constituent of both AC. The weak and broad diffraction peak  
393 ( $2\theta = 40-50^\circ$ ) is due to the a-axis of the graphite structure [35].

394 The intensity of the base line  $I_{am}$  of the diffractogram is mainly related to the presence of non-  
395 aromatic amorphous carbon in char [36].

396 The peak (100) is attributed to graphite structures in the plane [37] and reflects the size of the  
397 aromatic strata [38]. More the peak is narrower, the degree of condensation of the aromatic  
398 rings is high.

399 The peak (002) is attributed to the inter-reticular distance between the graphitic planes of the  
400 crystallites present in the char [339]. Theoretically, this peak is symmetrical. However, several  
401 studies have shown that an asymmetry characterized by the appearance of a shoulder on the left  
402 side of the peak (called the  $\gamma$  band) can reflect the presence of a stack of saturated structures  
403 such as aliphatic chains [40]. The region between 8 and 35 ° is therefore composed of two  
404 peaks (002) and  $\gamma$  band.

405 Diffractograms of sulfonated AC consist of two peaks corresponding to graphite planes (002)  
406 and (100). Suggesting that the chemical process does not affect the internal structure of carbon  
407 materials, this is consistent with many other reports, independently of the nature of the carbon  
408 used [41]. However, diffractograms of sulfonated AC show slight differences in the shapes and  
409 intensities of peaks:

- 410 - A shift of baseline signal indicating a drop in non-aromatic amorphous carbon concentration.
- 411 - Peak (100) became narrower after sulfonation revealing an increase in the condensation  
412 degree of aromatic cycles,
- 413 - Peak (002) became more symmetrical unveiling a decrease in the aliphatic carbon content.

414 Therefore, activated carbon becomes more aromatic under the effect of the sulfonation. The  
415 aliphatic carbon content (characterized by the  $\gamma$  band) has decreased because these structures  
416 weakly bound to the crystallites of char are removed as volatile compounds during the  
417 treatment with sulfuric acid. The treatment with H<sub>2</sub>SO<sub>4</sub> has caused a tightening of the peak  
418 (002) which also results in a decrease in the inter-reticular distance  $d_{002}$  or a higher crystallite

419 size. This evolution reflects the rise of carbon structure order and is in agreement with the  
420 literature data [42].

#### 421 3.2.4. Fourier Transform Infrared Spectroscopy (FT-IR):

422 The chemical nature of surface functionalities of OPAC, OPACS, CHAC and CHACS were  
423 investigated using FTIR analysis. Spectra of different samples are shown in Fig 4.

424 The most important absorption bands at frequency values were: OH stretching in hydroxyl  
425 groups (between  $3135\text{ cm}^{-1}$  and  $3445\text{ cm}^{-1}$ ), C-O stretch vibration ( $196$  and  $1636\text{ cm}^{-1}$ ), C-H  
426 deformation vibration ( $1384\text{ cm}^{-1}$ ) and the specific spectral bands of sulfur are compatible with  
427 S=O and S-O stretching in sulfonic acid such as  $\text{SO}_3\text{H}$  and sulfates  $\text{SO}_4^{2-}$  [43]. The detection of  
428 the sulfonic acid is usually located in the wavenumber ranges  $1080\text{-}1204\text{ cm}^{-1}$ . Whereas  
429 sulfates will appear between  $833$  and  $458\text{ cm}^{-1}$ [43].

430 Changes in the relative intensity of bands, particularly for those located at around  $1200\text{ cm}^{-1}$ ,  
431 indicate a greater presence of the sulfonic acid in OPACS. These results support the results  
432 found in ultimate and proximate analysis, which explains the percentage of oxygen that  
433 increases due to the formation of the sulfonic acid.

#### 434 3.2.5. Scanning Electron Microscopy (SEM):

435 Fig 5. presents SEM photographs of OPAC and CHAC before and after the sulfonation. Fig 5A  
436 and 5E show that OPAC and CHAC are composed of particles with varied morphologies and  
437 textures. OPAC particles are compact, differing with CHAC that are disorganized.

438 This is due to the anatomical orientation of the raw material, studies on the lignin distribution  
439 and the anatomical characteristics of the coconut and olive nut fibers were elaborated by Abdul  
440 K. *et al.* [44], These studies show that lignin is found in the cell walls of fibers, and that the  
441 olive nucleus has a much more compact structure without having phloems and meta-xylem.

442 which explains its compact morphology in fig (5A), in contrast to coconut, as phloems and  
443 meta-xylem, give it a more disordered structure.

444 Sulfonation has significantly modified char surface. Indeed, the OPACS has a mineral layer  
445 covering the vast majority of its surface (Fig 5B). This modification is very clear on the SEM  
446 images where mineral species appear brighter than the carbon matrix. While CHACS surface  
447 appears more orderly and more uniform. As mentioned before, capillary vessels, according to  
448 their functional botanical characteristics, leave voids in the structure of the raw material, which  
449 favors the development pores in the produced activated carbons.

450 Impregnation with  $H_2SO_4$  takes advantage of the disordered, porous structure of the activated  
451 carbon to ensure rapid and uniform diffusion, which significantly reduces the presence of voids  
452 in the sulfonated activated carbon and gives it this uniform filamentous appearance [25]. This  
453 morphology is already observed in agricultural wastes treated with sulfuric acid [45].

454 SEM images of OPAC and OPACS fig (5C and 5D), show lots of changes in the morphology  
455 of the activated carbon as a result of sulfonation procedure. These changes consist mainly on  
456 the purification of activated carbon, by eliminating impurities such as tar stuck in the  
457 micropores, which gives the surface a more homogeneous appearance. This observation is in  
458 line with the increase of BET surface and mesoporosity of CHACS. The same aspect can be  
459 observed for CHAC and CHACS.

460 It is very important to note that the pore structure of activated carbon developed and modified  
461 during activation varies widely from one char to another and that pores of different shapes  
462 (cylindrical, conical or bottle-shaped) can be obtained. Bottle-like pores appear during  
463 pyrolysis. According to Gonzalez-Serrano E. et al. [46], during carbonization, there are certain  
464 minerals, that produce a plastic phase which facilitates its distribution in lignocellulosic  
465 materials and allows the generation of bottle-like pores [47]. Activation with  $H_2O$  vapor, allows

466 developing cone-shaped pores, generated by the gasification reactions of carbon, the pores have  
467 a conical shape due to the difference in H<sub>2</sub>O concentration in the carbon grain and the  
468 difference in reactivity of the carbon atoms. Bottle shaped and cone-shaped pores can be seen  
469 clearly in figs (5C and 5H) [48].

### 470 **3.3. Using sulfonated AC as catalyst for esterification**

#### 471 3.3.1. Turn Over Frequency of different catalysts

472 CHACS and OPACS were tested as catalysts for the methanolysis of FFA contained in olive  
473 pomace oil having an acidity of 126 mg<sub>KOH</sub>/g<sub>oil</sub>. Sulfuric acid was also used for comparison  
474 under conditions stated in authors research team's previous work [49]. The reaction  
475 advancement was followed with respect to time by analyzing the acidity of samples taken from  
476 the reactor each hour using different catalysts under different conditions

477 The results are presented in figure 6. As it can be noticed, two phases can be distinguished in  
478 the for different catalysts. A rapid phase where acid value (AV) decreases rapidly before  
479 arriving to a slow phase where the chemical equilibrium is approached. This observation is in  
480 line with those set by Stamenkovic et al. [50] who divided the kinetics of transesterification  
481 reaction following three consecutive phases. a mass transfer controlled one that is very short  
482 (few minutes) and can not be noticed at temperatures higher than 30°C with good agitation.  
483 Thus most studies deal with the reaction without taking it in account. While the chemically  
484 controlled phase can be divided into two pseudo-homogeneous parts. The first part is very fast  
485 while the second one, also called equilibrium phase is slow. The esterification process is very  
486 similar to transesterification due to the immiscibility of phases, the slow and the reversible  
487 character of the reaction and due to species entering in reaction. Thus the approach of  
488 Staminovic et al. could be representative of esterification also.

489 It can be noticed that the homogeneous catalysis has the highest conversion rate during the first  
490 phase of reaction ( $t < 1\text{h}$ ), while it has the lowest rate during the second one. The good  
491 miscibility of sulfuric acid with other reagents gives a better performance at the beginning of  
492 the reaction, but the accumulation of water started to slow down the reaction because of the  
493 reverse reaction. Furthermore, the solubility of sulfuric acid in water leads to its dissociation  
494 and deactivation. On the other hand, AC-based heterogeneous catalysts are hydrophobic which  
495 allows them to absorb methanol and lipids and to repel water formed during reaction. Thus  
496 reaction medium around  $\text{SO}_3\text{H}$  sites are more favorable for direct reaction than reverse one  
497 which explains why these catalysts have steeper slopes at advanced stages of reaction.

498 OPACS and CHACS have similar trends during the first hour of reaction with higher FFA  
499 conversion rates registered for CHACS. During the second period ( $t > 1\text{h}$ ) the trends are shifted  
500 and the OPACS results with fastest FFA conversion. The higher rate noticed with CHACS  
501 during the first stage of reaction could be related to its higher surface area and mesoporous  
502 volume (almost twice of those of OPACS) which allows a faster diffusion of reagents inside its  
503 pores, especially that the mixture has a high viscosity at this phase. During the second phase ( $t$   
504  $> 1\text{h}$ ) the highest content of  $\text{SO}_3\text{H}$  of OPACS leads to a better reaction rate despite its lower  
505 surface area and mesoporous volume. In fact, with reaction advancement, more FFA are  
506 transformed to methyl esters and the viscosity of the mixture becomes lower which reduces the  
507 effect of mass transfer on reaction.

508 The trend of reaction with homogeneous and heterogeneous catalysts fits well with the  
509 observations of Staminovic et al. with a very fast phase followed by a very slow one.  
510 Concerning the fast phase, reaction using OPACS is significantly slower than those using  
511 CHACS and Sulfuric acid as catalysts. In fact, the oil has lost 87% of its AV using  
512 homogeneous catalyst during the first hour of reaction. The decrease in AV during the first  
513 hour of reaction has also ranged between 72% (3:1, 10%) and 85.5% (9:1, 20%) when using

514 CHACS. While the use of OPACS resulted in a decrease of AV during the first hour ranging  
515 between 61% (3:1, 10%) and 73.2% (9:1, 20%).

516 However, after 5 h of reaction OPACS and CHACS resulted on similar AV conversion ranging  
517 between 75% and 99% with a slightly higher conversion for CHACS.

518 In order to analyze the performance of different catalysts, turn over frequency (TOF) was  
519 compared for different catalysts under different conditions after 1h (TOF<sub>1h</sub>) and 5 h (TOF<sub>5h</sub>) of  
520 reaction, respectively. Results are presented in Table 3. It can be clearly noticed that the  
521 reaction is very fast during the first phase where the TOF<sub>1h</sub> is on average 3.6 times and 4.2  
522 times higher than TOF<sub>5h</sub> for OPACS and CHACS respectively.

523 On the other hand, it is obvious that the CHACS has the highest efficiency per acid site,  
524 followed by OPACS then by Sulfuric acid. When compared at same conditions, the TOF<sub>5h</sub> of  
525 CHACS is on average 3.15 times higher than that of OPACS. This ratio corresponds almost to  
526 the ratio of sulfur content of OPACS divided by that of CHACS (3.133). That means that the  
527 deficiency in acid sites was compensated by other aspects of the CHACS such as its mesopores  
528 content that is twice that of OPACS. At the same time TOF<sub>1h</sub> for CHACS is on average 3.7  
529 times higher than that of CHACS which exceeds the ratio of sulfur contents. This observation  
530 means that during the first phase the mass transfer through the pores of catalyst has a very  
531 important role in the reaction.

532 TOF<sub>1h</sub> and TOF<sub>5h</sub> of OPACS are 2.6 - 4.6 times and 3 - 6 times higher than that of sulfuric acid,  
533 respectively, at same methanol to FFA molar ratio. This can be explained by the  
534 hydrophobicity of the activated carbon that repels water from reaction zone which enhances  
535 reaction kinetics and preserves acid sites from dissociation. The highest TOF<sub>5h</sub> of OPACS to  
536 sulfuric acid ratio as compared to that of TOF<sub>1h</sub> indicates that mass transfer in catalysts pores  
537 has a higher effect during the first hour of reaction.

538 For both heterogeneous catalysts  $TOF_{1h}$  and  $TOF_{5h}$  are inversely proportional to catalyst  
 539 loading. For instance, at constant molar ratio, increasing catalyst loading from 10% to 15% and  
 540 to 20% divides TOF by almost 1.5 and 2 times respectively. These ratios are getting closer to  
 541 1.5 and 2 with the increase of molar ratio and reaction time. These trends reveal that increasing  
 542 the catalyst loading does not bring lots of enhancement to the reaction output in terms of  
 543 conversion. However, the stringent limit of  $2 \text{ mg}_{KOH}/\text{g}_{oil}$  makes the slight increase in  
 544 conversion rates due to catalyst load increase meaningful.

545 At the same extent, increasing methanol to FFA ratio brings around 0.97% and 0.95%  
 546 enhancement in  $TOF_{5h}$  per additional mole of methanol per mole of FFA for OPACS and  
 547 CHACS respectively. This trend could be explained by the enhancement of reaction kinetics  
 548 and the diffusion of reactive mixture inside catalyst pores due to lower viscosity.

### 549 3.3.2. Kinetic study

550 In order to shed lights on the second phase of reaction ( $t > 1 \text{ h}$ ) of reaction where it is meant to  
 551 reach its equilibrium, it is suggested to lead a kinetic study. Among different models suggested  
 552 in literature an irreversible, pseudo-first order kinetic model gave the best fit. Esterification  
 553 reaction is presented in equation 8:



555 The rate of reaction can be then expressed as in equation 9

$$556 \quad \frac{dFFA}{dt} = -k_1 FFA \cdot M + k_2 ME \cdot W \quad (9)$$

557 For an irreversible reaction  $k_2$  is set to zero, while for a pseudo-first order reaction, the excess  
 558 of alcohol is considered sufficiently high to consider that methanol concentration is constant  
 559 during the reaction [51]. Thus equation 9 can be transformed to equation 10:

$$560 \quad \frac{dFFA}{dt} = -k \cdot FFA \quad (10)$$

561 Where  $k = M_0 \cdot k_1$ . With  $M_0$  is the methanol concentration at the beginning of reaction. FFA in  
 562 equation 10 can be replaced by acid value AV since  $FFA = m_{oil} \cdot AV / M_{KOH}$  where  $m_{oil}$  is the  
 563 mass of oil used in the reaction and  $M_{KOH}$  is molar mass of KOH.

564 Using the integral method on the segment ( $t > 1$  h) of the curve, the rate constant of reaction  
 565 was determined for all experiments led with all of three catalysts at different operating  
 566 conditions. Results are presented in Table 4. Rate constants are higher when using OPACS with  
 567 respect to CHACS and to homogeneous catalysts. At similar conditions k value when using  
 568 OPACS is 1.11 to 1.85 times higher than that of CHACS which is lower than the ratio between  
 569 sulfur (catalytic sites) contents of both catalysts. This means that the mass transfer through the  
 570 pores and the hydrophobicity of catalysts are playing important roles. The mesopores of  
 571 CHACS increase the mass transfer inside the catalyst and thus compensate the lower number of  
 572 acid sites while its hydrophobicity repels formed water during reaction and enhances species  
 573 balance around acid sites and approaches more the irreversible reaction model. Rate constants  
 574 have increasing trends with the increase of alcohol:oil ratio and with catalyst loading and they  
 575 vary in a linear way with both parameters. The increasing trend with catalyst loading is related  
 576 to the increase in catalytic sites density. This trend was observed in different studies where  
 577 increasing catalyst load increases activation energy and/or pre-exponential factor [52 - 54].  
 578 Increasing k with methanol loading is related to 2 aspects, the first one is obvious from  
 579 equation 10 where  $k = M_0 \cdot k_1$  while the second aspect is related to the decrease in mixtures  
 580 viscosity which enhances mass transfer inside pores. In the case of CHACS, passing from a  
 581 molar ratio of 3:1 to 6:1 and to 9:1 multiplies k by 2.3 times and 3.1 times on average,  
 582 respectively. These values are 10 – 30% higher to what is expected by equation 10. In the case  
 583 of OPACS, multiplying molar ratio by 2 and 3 times multiplies k by 1.6 times and 2.3 times on

584 average, respectively. These trends are 20-25% lower from what is expected based on  
585 equation 10. These deviations from the suggested model could be related to the effects of mass  
586 transfer of reagents through the pores of catalyst. Further investigations are needed in order to  
587 take in consideration the mass transfer through the pores and it could not be covered in the  
588 present work.

### 589 *3.3.3. Final product characterization*

590 At the highest loading of catalyst and methanol the acid value has reached 1.14 mg<sub>KOH</sub>/g using  
591 CHACS and 1.41 mg<sub>KOH</sub>/g using OPACS. Although the highest rate during the second part of  
592 reaction, CHACS exhibited a slightly highest FFA conversion rate, which emphasizes the  
593 importance of the first phase of reaction. GC-FID analysis of the product obtained using  
594 OPACS (9:1, 20%) has shown very low contents of mono, di, and triglycerides (0.4, 0.8 and 0  
595 %) respectively with a viscosity of 3.02 mm<sup>2</sup>/s at 40°C. At the same time, GC-MS has shown a  
596 FAME content of 97.3%. Thus, it could be concluded that the used catalyst is able at the same  
597 time to catalyze esterification and transesterification processes. A further optimization could be  
598 needed in order to decrease FFA and diglycerides contents to meet EN14214 requirements  
599 (0.5 mg<sub>KOH</sub>/g and 0.2 % respectively) [55]. This would avoid a second step of reaction.

## 600 **4- Conclusions**

601 In this study, solid acid catalyst was produced from olive pomace-based activated carbon by  
602 sulfonation. Commercial activated carbon was also used for comparison. Catalysts were  
603 characterized and used for the esterification of olive pomace oil (OPO).

604 Olive pomace was first pyrolyzed before undergoing an activation with superheated steam. The  
605 resulting product is an activated carbon (OPAC) with a moderate specific surface dominated by  
606 micropores. The sulfonation of OPAC increased the BET surface and the specific pore volume  
607 by 80% and 36% respectively by cleaning pores from residual tar and by enlarging micropores.

608 This result was confirmed by XRD and SEM analysis. The final product was rather  
609 microporous. Almost same results were obtained with commercial coconut husk based  
610 activated carbon (CHAC) that was rather mesoporous.

611 Although its higher specific surface and porosity, CHAC fixed 70% less sulfur than OPAC.  
612 This observation could be attributed to the lower hydrophobicity of the latter that allows a  
613 better wetting of surfaces, leading to better impregnation of sulfur. FTIR spectroscopy has  
614 shown that sulfur was mainly fixed in form of sulfonic acid in both catalysts, with lower peaks  
615 corresponding to sulfates.

616 Esterification reaction was then performed using both catalysts and were compared to  
617 homogeneous catalysis using sulfuric acid. Reaction order and rate constants were  
618 determined under different operating conditions. Two phases of were distinguished. During  
619 the first phase homogeneous catalysis is more efficient and FFA are converted faster.  
620 During the second phase heterogeneous catalysts have a faster rate.

621 CHACS has a better performance during the first phase as compared to OPACS. While the  
622 latter exhibits faster kinetics during second phase. Turn over frequencies (TOF) of different  
623 catalysts were studied and after 5 h of reaction it turns out that both catalysts give similar  
624 performances although the differences in acid sites densities and mesoporous volumes.  
625 Increasing methanol to FFA molar ratio has increased TOF by almost 1% per mol of  
626 methanol:mol FFA.

627 The second phase of reaction was modeled as a direct first order reaction. At different  
628 conditions the suggested model gave a good fit. Some deviations were noticed concerning  
629 the effect of methanol:FFA ration the rate constant evolution. Mass transfer through pores  
630 could be responsible of this deviation. A more detailed mechanistic study could reveal its  
631 exact effects.

632 The highest methanol and catalyst loading gave higher FFA conversion rates. When using  
633 9:1 methanol:oil molar ratio and 20% catalyst load, both heterogeneous catalysts gave place  
634 to acid values lower than 2 mg<sub>KOH</sub>/g. GC-FID/MS analysis of the one obtained using  
635 OPACS showed that its di-glycerides content is slightly higher than the requirements of  
636 EN14214, while mono and triglycerides respect them with a content of fatty acids methyl  
637 esters Higher than 97%. The viscosity was also measured and it recorded 3 mm<sup>2</sup>/s.

638

### 639 **References:**

- 640 [1]. M. V. Lopez-ramon, C. Moreno-castilla, F. Carrasco-marín, and M. A. Alvarez-merino,  
641 “Chemical and physical activation of olive-mill waste water to produce activated carbons,” vol.  
642 39, pp. 1415–1420, 2001.
- 643 [2]. P. Vossen, “Olive Oil : History , Production , and Characteristics of the World ’ s Classic Oils,”  
644 vol. 42, no. 5, pp. 1093–1100, 2007.
- 645 [3]. J. C. Jose Antonio Albuquerque, J González, Dumeivy Garcia, “Agrochemical  
646 characterisation of ‘Alperujo’, a solid by-product of the two-phase centrifugation method for  
647 olive oil extraction,” *Bioresource Technology*, pp. 195–200, 2004.
- 648 [4]. B. Leblon et al., *SUSTAINABLE DEVELOPMENT – AUTHORITATIVE AND LEADING*  
649 *EDGE CONTENT FOR ENVIRONMENTAL* Edited by Sime Curkovic. 2012.
- 650 [5]. M.-G. J. Jauhiainen, J.A. Conesa, R. Font, “Kinetics of the pyrolysis and combustion of olive  
651 oil solid waste,” *Journal of analytical and applied pyrolysis*, 2004.
- 652 [6]. C. Russo et al., “Product environmental footprint in the olive oil sector : State of the art,”  
653 *Environmental Engineering and Management Journal*, . Vol.15, No. 9, 2019-2027 .
- 654 [7]. F. Cheng and X. Li, “Preparation and Application of Biochar-Based Catalysts for Biofuel  
655 Production,” no. 1, pp. 1–35, 2018.

- 656 [8]. J. R. Kastner, J. Miller, D. P. Geller, J. Locklin, L. H. Keith, and T. Johnson, "Catalytic  
657 esterification of fatty acids using solid acid catalysts generated from biochar and activated  
658 carbon," *Catalysis Today*, vol. 190, no. 1, pp. 122–132, 2012.
- 659 [9]. T. Liu, Z. Li, W. Li, C. Shi, and Y. Wang, "Preparation and characterization of biomass carbon-  
660 based solid acid catalyst for the esterification of oleic acid with methanol," *Bioresource  
661 Technology*, vol. 133, pp. 618–621, 2013.
- 662 [10]. S. Dora, T. Bhaskar, R. Singh, D. V. Naik, and D. K. Adhikari, "Effective catalytic  
663 conversion of cellulose into high yields of methyl glucosides over sulfonated carbon based  
664 catalyst," *Bioresource Technology*, vol. 120, pp. 318–321, 2012.
- 665 [11]. M. Dehkoda, A. H. West, and N. Ellis, "Biochar based solid acid catalyst for biodiesel  
666 production," *Applied Catalysis A, General*, vol. 382, no. 2, pp. 197–204, 2010.
- 667 [12]. ASTM D3175-20, Standard Test Method for Volatile Matter in the Analysis Sample of  
668 Coal and Coke, ASTM International, West Conshohocken, PA, 2020
- 669 [13]. F. Kifani-sahban, L. Belkbir, and A. Zoulalian, "Study of the slow pyrolysis of  
670 Moroccan eucalyptus by thermal analysis," 1996, *thermochimica acta*.
- 671 [14]. ASTM D1102-84(2013), Standard Test Method for Ash in Wood, ASTM International,  
672 West Conshohocken, PA, 2013
- 673 [15]. ASTM D3174-12(2018), Standard Test Method for Ash in the Analysis Sample of Coal  
674 and Coke from Coal, ASTM International, West Conshohocken, PA, 2018
- 675 [16]. ASTM D664-18e2, Standard Test Method for Acid Number of Petroleum Products by  
676 Potentiometric Titration, ASTM International, West Conshohocken, PA, 2018A
- 677 [17]. Naoko Ellis, Feng Guan, Tim Chen, Conrad Poon, Monitoring biodiesel production  
678 (transesterification) using in situ viscometer, *Chemical Engineering Journal* 138 (2008) 200–  
679 206.
- 680 [18]. Ayhan Demirbad, Relationships derived from physical properties of vegetable oil and  
681 biodiesel fuels, *Fuel* 87 (2008) 1743–1748

- 682 [19]. ): EN ISO 3104 (1994) Petroleum products — Transparent and opaque liquids —  
683 Determination of kinematic viscosity and calculation of dynamic viscosity, PR NF EN ISO  
684 3104
- 685 [20]. G. Leofanti, M. Padovan, G. Tozzola, B. Venturelli, Surface area and pore texture of  
686 catalysts, *Catal. Today*. 41 (1998) 207–219. doi:10.1016/S0920-5861(98)00050-9.
- 687 [21]. K.S.W. Sing, D.H. Everett, R.a.W. Haul, L. Moscou, R.a. Pierotti, J. Rouquerol,  
688 T.Siemieniewska, International union of pure commission on colloid and surface chemistry  
689 including catalysis\* Reporting physisorption data for gas/solid systems with special reference to  
690 the determination of surface area and porosity, *Pure Appl. Chem.* 54 (1982) 2201-2218.
- 691 [22]. L. A. De Macedo, “Torréfaction de biomasse lignocellulosique : effet catalytique du  
692 potassium sur les espèces condensables Université de Lorraine, 2018.
- 693 [23]. S. Zellagui, “Pyrolyse et combustion de solides pulvérisés sous forts gradients  
694 thermiques : Caractérisation de la dévolatilisation , des matières particulaires générées et  
695 modélisation ” université haute-alsace, 2017.
- 696 [24]. U. Arena, “Process and technological aspects of municipal solid waste gasification . A  
697 review,” *Waste Management*, vol. 32, no. 4, pp. 625–639, 2012.
- 698 [25]. M. J. Prauchner and F. Rodríguez-reinoso, “Chemical versus physical activation of  
699 coconut shell : A comparative study,” *Microporous and Mesoporous Materials*, vol. 152, pp.  
700 163–171, 2012.
- 701 [26]. L. Medouni-haroune, F. Zaidi, S. Medouni-adrar, and M. Kecha, “Olive pomace: from  
702 an olive mill waste to a resource, an overview of the new treatments” *Journal of Critical*  
703 *Reviews*, vol. 5, no. 6, pp. 1–6, 2018.
- 704 [27]. V. Skoulou and A. Zabaniotou, “Investigation of agricultural and animal wastes in  
705 Greece and their allocation to potential application for energy production,” *Renewable and*  
706 *Sustainable Energy Reviews*, no. January 2018, 2007.
- 707 [28]. R. Zanzi, K. Sjoström, and E. Bjornbom, “Rapid pyrolysis of agricultural residues at  
708 high temperature,” *Biomass and Bioenergy*, vol. 23, pp. 357–366, 2002.

- 709 [29]. P. Fu et al., "Structural evolution of maize stalk / char particles during pyrolysis,"  
710 Bioresource Technology, vol. 100, no. 20, pp. 4877–4883, 2009.
- 711 [30]. V. E. Diyuk, R. T. Mariychuk, and V. V Lisnyak, "Functionalization of activated  
712 carbon surface with sulfonated styrene as a facile route for solid acids preparation," Materials  
713 Chemistry and Physics, vol. 184, pp. 138–145, 2016.
- 714 [31]. M. N. Alaya, M. A. Hourieh, A. M. Youssef, and F. E. F. Science, "Adsorption  
715 Properties of Activated Carbons Prepared from Olive Stones," Adsorption Science and  
716 Technology, vol. 1, no. 1, pp. 27–42, 1999.
- 717 [32]. Kumar and H. M. Jena, "High surface area microporous activated carbons prepared  
718 from Fox nut ( *Euryale ferox* ) shell by zinc chloride activation," Applied Surface Science, vol.  
719 356, pp. 753–761, 2015.
- 720 [33]. L. Tang, L. Li, R. Chen, C. Wang, W. Ma, and X. Ma, "Adsorption of acetone and  
721 isopropanol on organic acid modified activated carbons," Biochemical Pharmacology, vol. 4,  
722 no. 2, pp. 2045–2051, 2016.
- 723 [34]. D. D. Do, S. Junpirom, and H. D. Do, "A new adsorption – desorption model for water  
724 adsorption in activated carbon," Carbon, vol. 47, no. 6, pp. 1466–1473, 2009.
- 725 [35]. S. Suganuma, K. Nakajima, M. Kitano, and D. Yamaguchi, "Hydrolysis of Cellulose by  
726 Amorphous Carbon Bearing SO<sub>3</sub>H, COOH, and OH Groups," Journal of the American  
727 Chemical Society, pp. 12787–12793, 2008.
- 728 [36]. P. Fu, W. Yi, X. Bai, Z. Li, S. Hu, and J. Xiang, "Effect of temperature on gas  
729 composition and char structural features of pyrolyzed agricultural residues," Bioresource  
730 Technology, vol. 102, no. 17, pp. 8211–8219, 2011.
- 731 [37]. M. Guerrero, M. P. Ruiz, Á. Millera, M. U. Alzueta, and R. Bilbao, "Characterization of  
732 Biomass Chars Formed under Different Devolatilization Conditions : Differences between Rice  
733 Husk and Eucalyptus," Energy & Fuels, no. 17, pp. 1275–1284, 2008.
- 734 [38]. M. Shahed et al., "Production, characterization and reactivity studies of chars produced  
735 by the isothermal pyrolysis of flax straw," Biomass and Bioenergy, vol. 37, pp. 97–105, 2011.

- 736 [39]. P. Lahijani, Z. Alimuddin, A. Rahman, and M. Mohammadi, "CO<sub>2</sub> gasification  
737 reactivity of biomass char : Catalytic influence of alkali , alkaline earth and transition metal  
738 salts," *Bioresource Technology*, vol. 144, pp. 288–295, 2013.
- 739 [40]. L. Lu, C. Kong, V. Sahajwalla, and D. Harris, "Char structural ordering during  
740 pyrolysis and combustion and its influence on char reactivity q," *FUEL*, vol. 81, pp. 1215–  
741 1225, 2002.
- 742 [41]. D. Vamvuka, S. Troulinos, and E. Kastanaki, "The effect of mineral matter on the  
743 physical and chemical activation of low rank coal and biomass materials," *FUEL*, vol. 85, pp.  
744 1763–1771, 2006.
- 745 [42]. B. Manoj and A. G. Kunjomana, "Study of Stacking Structure of Amorphous Carbon by  
746 X-Ray Diffraction Technique," *International Journal of electrochemical science*, vol. 7, pp.  
747 3127–3134, 2012.
- 748 [43]. R. Conley, "In Espectroscopia Infrarroja.," 1979, vol. pp. 203-10.
- 749 [44]. Á. López-bernal, E. Alcántara, L. Testi, and F. J. Villalobos, "Spatial sap flow and  
750 xylem anatomical characteristics in olive trees under different irrigation regimes," *Tree  
751 Physiology*, pp. 1536–1544, 2010.
- 752 [45]. Kula, M. Ug, C. Ali, and H. Karaog, "Adsorption of Cd ( II ) ions from aqueous  
753 solutions using activated carbon prepared from olive stone by ZnCl<sub>2</sub> activation," *Bioresource  
754 Technology*, vol. 99, pp. 492–501, 2008.
- 755 [46]. J. J. Rodri, "Development of Porosity upon Chemical Activation of Kraft Lignin with  
756 ZnCl<sub>2</sub>," *Ind. Eng. Chem. Res.*, pp. 4832–4838, 1997.
- 757 [47]. Harry Marsh Francisco Rodríguez Reinoso, "Activated Carbon", Ed. Elsevier, Great  
758 Britain, ISBN: 9780080444635. 2006.
- 759 [48]. C. E. De la Torre E., Guevara A., *Revista Politécnica, EPN*, 27-2, P.53. 2007.
- 760 [49]. S. Awad, M. Paraschiv, E. G. Varuvel, and M. Tazerout, "Bioresource Technology  
761 Optimization of biodiesel production from animal fat residue in wastewater using response  
762 surface methodology," *Bioresource Technology*, vol. 129, pp. 315–320, 2013.

- 763 [50]. O.S. Stamenkovic, Z.B. Todorovic, M.L. Lazic, V.B. Veljkovic, D.U. Skala, Kinetics of  
764 sunflower oil methanolysis at low temperatures, *Bioresour. Technol.* 98 (2007) 1131–1140.
- 765 [51]. Matthieu Tubino, José Geraldo Rocha Junior, Glauco Favilla Bauerfeldt, Biodiesel  
766 synthesis with alkaline catalysts: A new refractometric monitoring and kinetic study, *Fuel* 125  
767 (2014) 164–172
- 768 [52]. M. Berrios, J. Siles, M.A. Martín, A. Martín, A kinetic study of the esterification of  
769 free fatty acids (FFA) in sunflower oil, *Fuel* 86 (2007) 2383–2388
- 770 [53]. Chia-Hung Su, Kinetic study of free fatty acid esterification reaction catalyzed by  
771 recoverable and reusable hydrochloric acid, *Bioresource Technology* 130 (2013) 522–528
- 772 [54]. Thanh Lieu, Suzana Yusup, Muhammad Moniruzzaman, Kinetic study on microwave-  
773 assisted esterification of free fatty acids derived from *Ceiba pentandra* Seed Oil, *Bioresource*  
774 *Technology* 211 (2016) 248–256
- 775 [55]. Committee for Standardization Automotive fuels—fatty acid methyl esters (FAME) for  
776 diesel engines—requirements and test methods. European Committee for Standardization,  
777 Brussels; 2003a. Method EN 14214.

778

Table 1: Ultimate and Proximate Analysis

Biomass samples	Ultimate Analysis (wt %)				Proximate Analysis		
	% N	% C	% H	% S	% O	Ash	Volatile's yield
Olive pomace	0.82	45.31	5.54	LD	41.51	0.32	71.15
Bio-char	1.06	77.95	1.76	LD	4.41	7.88	
Sulfonated Bio-char	3.25	65.66	1.60	LD	7.38	8.45	
OPAC	0.43	85.14	0.86	LD	1.98	8.48	
OPACS	0.33	75.0	1.22	3.54	10.95	8.95	
CHAC	LD	90.05	0.38	LD	1.52	7.99	
CHACS	LD	87.73	0.77	1.13	6.12	8.44	

Results expressed in% by mass

*LD* : lowest than the limit of detection ( $LD < 0,06$  % on *CHNS-O*)

*OPAC*: Olive Pomace Activated Carbon

*OPACS*: Sulfonated Olive Pomace Activated Carbon

*CHAC*: Coconut Husk Activated Carbon

*CHACS*: Sulfonated Coconut Husk Activated Carbon

*Table 2: Physical characteristics of solid acid carbon catalysts*

Samples	Surface area <sup>a</sup> (m <sup>2</sup> /g)	Total pore volume <sup>b</sup> (cm <sup>3</sup> /g)	Micropore <sup>*b</sup> Volume (cm <sup>3</sup> /g)	Mesopore <sup>*c</sup> volume (cm <sup>3</sup> /g)
<b>OPAC</b>	345.31 ± 4.91	0.240	0.106	0.125
<b>OPACS</b>	618.18 ± 9.18	0.328	0.203	0.074
<b>CHAC</b>	1227.01 ± 7.4646	0.542	0.380	0.001
<b>CHACS</b>	1379.91 ± 15.23	0.784	0.274	0.152

For Abbreviations please refer to table 1

\* Micro:  $D_p < 2$  nm; Meso:  $2 < D_p < 50$  nm; Macro:  $D_p > 50$  nm.

a: single point surface area at  $p/p^\circ = 0.290836494$  ; b: determined from t-plot model; c: determined from BJH adsorption pore distribution.

Table 3: TOF of esterification using OPACS, CHACS and sulfuric acid under different conditions

	OPACS			CHACS			H <sub>2</sub> SO <sub>4</sub>
Catalyst loading ►	10%	15%	20%	10%	15%	20%	3.6%
Methanol : oil molar ratio ▼	<b>TOF<sub>1h</sub> (h<sup>-1</sup>)/TOF<sub>5h</sub> (h<sup>-1</sup>)</b>						
<b>3 :1</b>	12.452/3.455	8.273/2.386	7.069/1.854	46.393/10.897	32.582/7.478	24.632/5.815	2.692/0.595
<b>6 :1</b>	12.797/3.740	8.729/2.524	7.105/1.957	46.154/11.834	33.602/8.136	25.300/6.144	-
<b>9 :1</b>	13.754/3.932	9.727/2.638	7.442/2.011	50.544/12.329	34.070/8.282	27.231/6.314	-

For Abbreviations please refer to table 1

Table 4: Constant rate of esterification using OPACS, CHACS and sulfuric acid under different conditions

	OPACS			CHACS			H <sub>2</sub> SO <sub>4</sub>
Catalyst loading ►	10%	15%	20%	10%	15%	20%	3.6%
Methanol : oil molar ratio ▼	<b>k (h<sup>-1</sup>)</b>						
<b>3 :1</b>	0.23598	0.294	0.304	0.143	0.158	0.207	0.275
<b>6 :1</b>	0.38111	0.432	0.522	0.332	0.390	0.437	-
<b>9 :1</b>	0.5681	0.604	0.784	0.445	0.502	0.668	-

For Abbreviations please refer to table 1

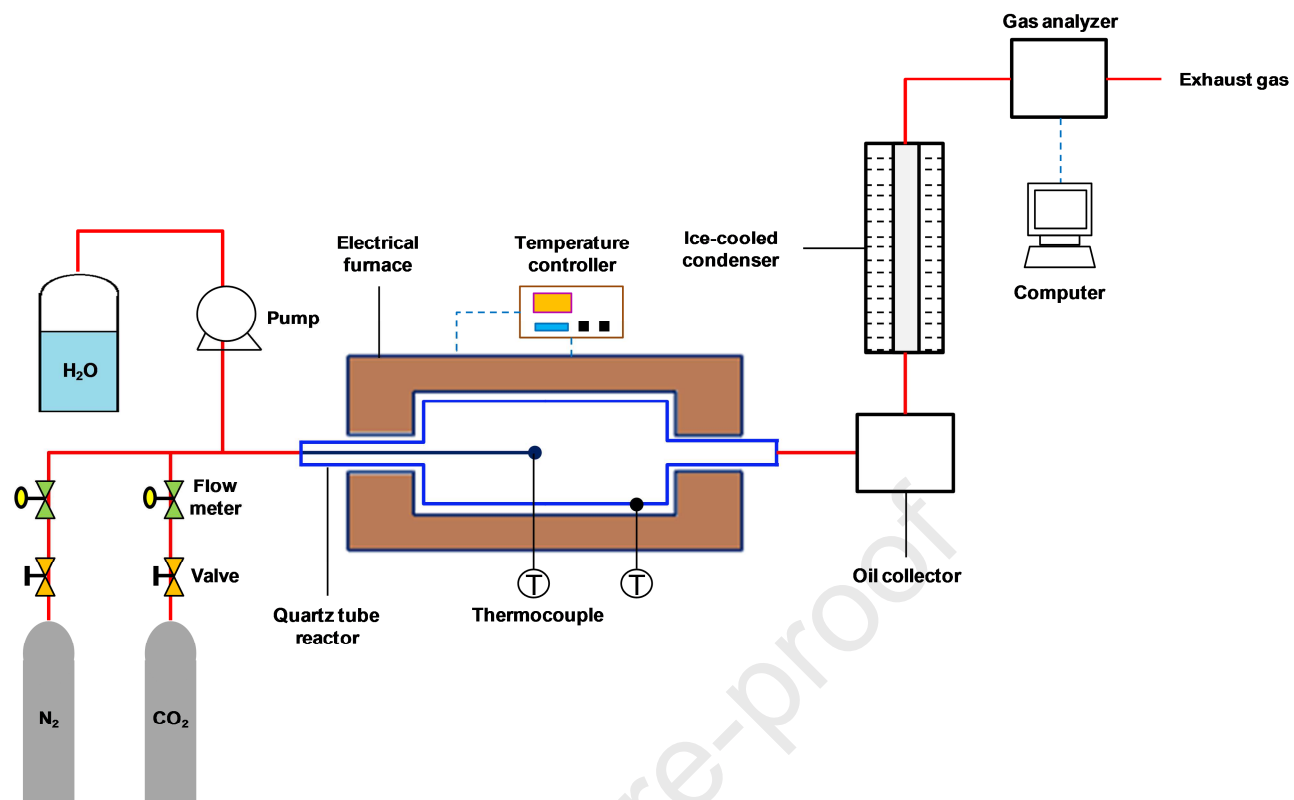


Fig. 1. Experimental set-up

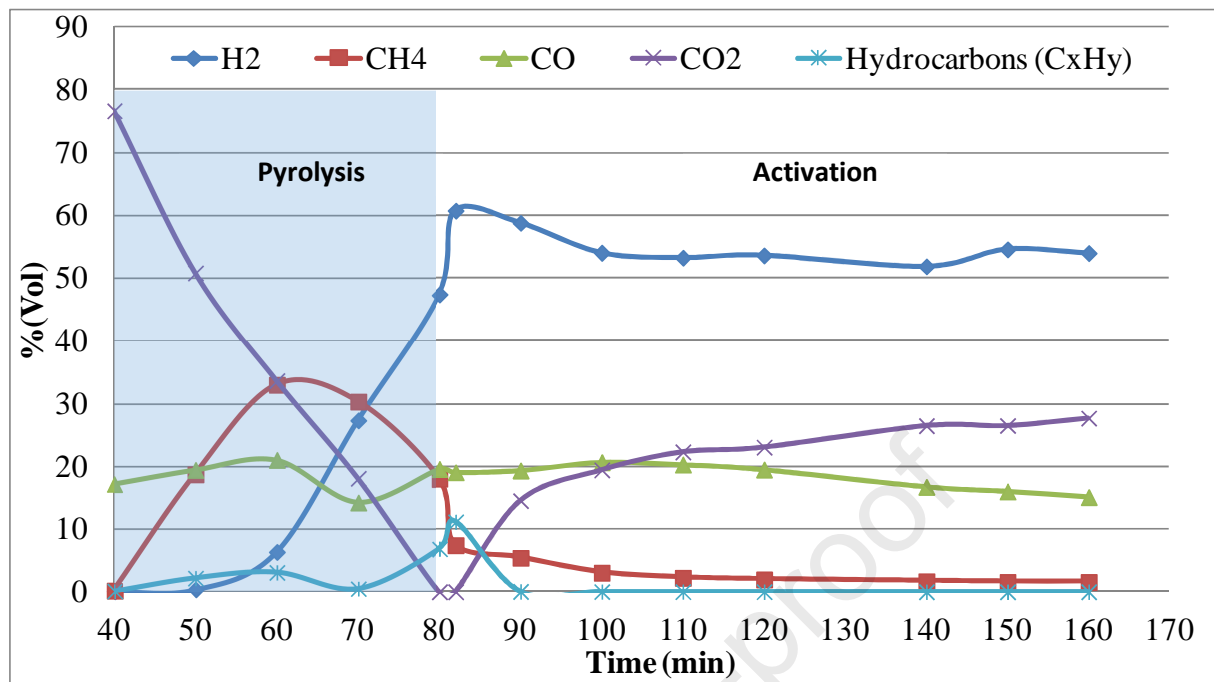


Fig. 2. Composition of gases produced during activation of olive pomace char

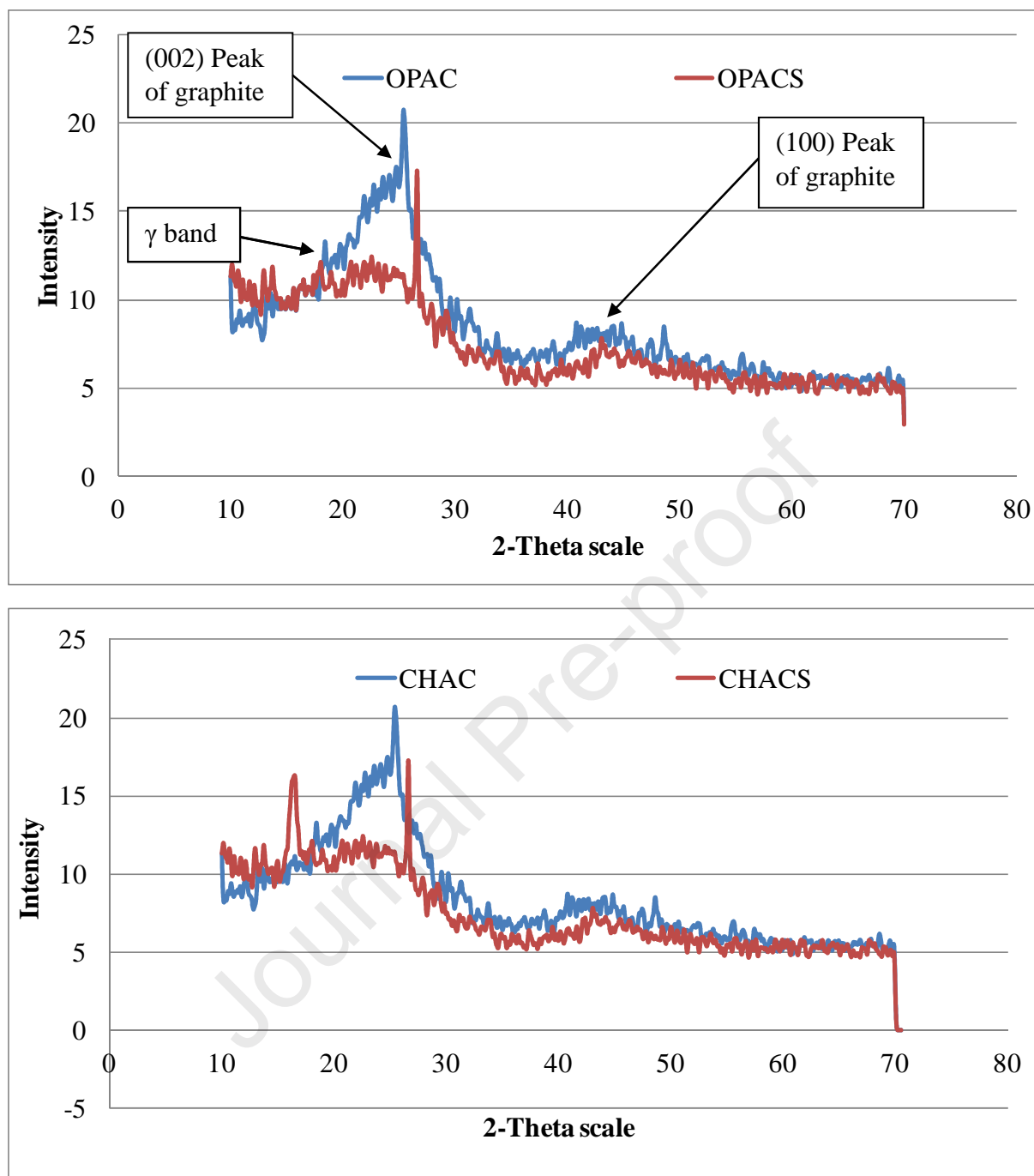


Fig. 3. Typical XRD patterns of the initial OPAC (olive pomace activated carbon), OPACS (sulfonated olive pomace activated carbon), CHAC (commercial coconut husk based activated carbon) and CHACS (sulfonated commercial coconut husk based activated carbon) samples

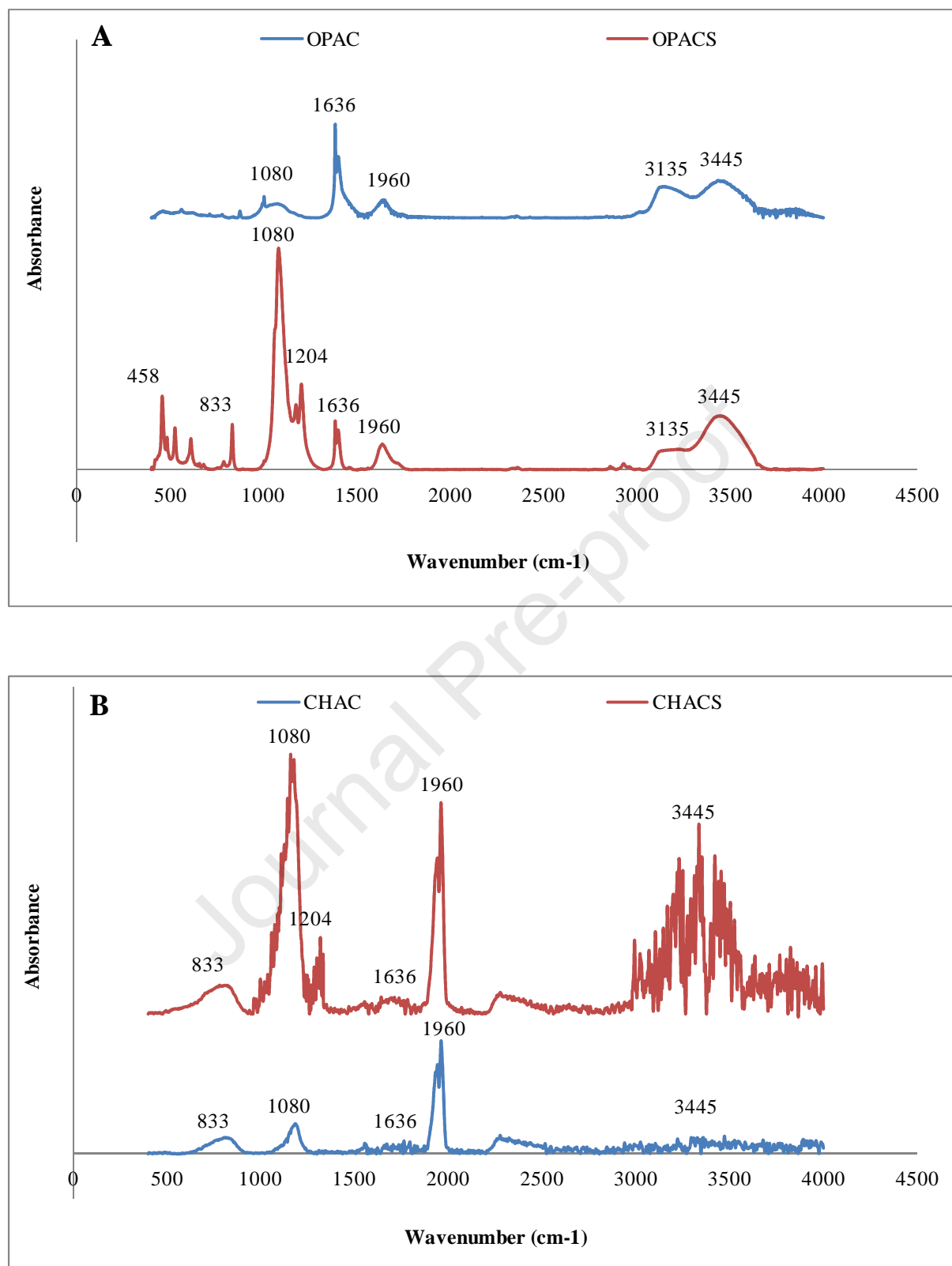


Fig. 4. Spectrum of FTIR analysis from (A): OPAC (olive pomace activated carbon) and OPACS (sulfonated olive pomace activated carbon) and (B): CHAC (commercial coconut husk based activated carbon) and CHACS (sulfonated commercial coconut husk based activated carbon)

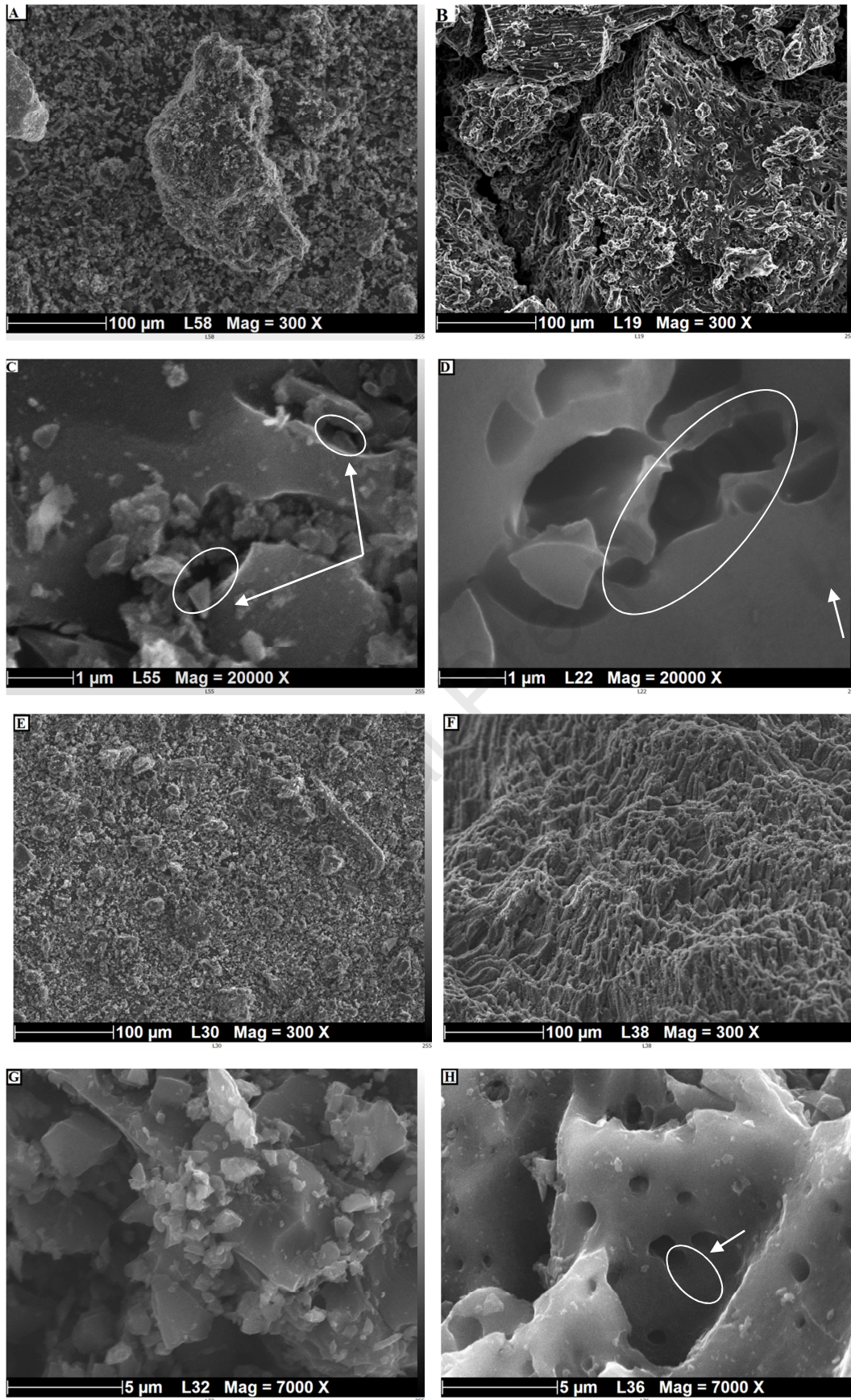


Fig. 5. SEM micrographs of (A and C) OPAC (olive pomace activated carbon), (B and D) OPACS (sulfonated olive pomace activated carbon), (E and G) CHAC (commercial coconut husk based

activated carbon) and (F and H) CHACS (sulfonated commercial coconut husk based activated carbon).

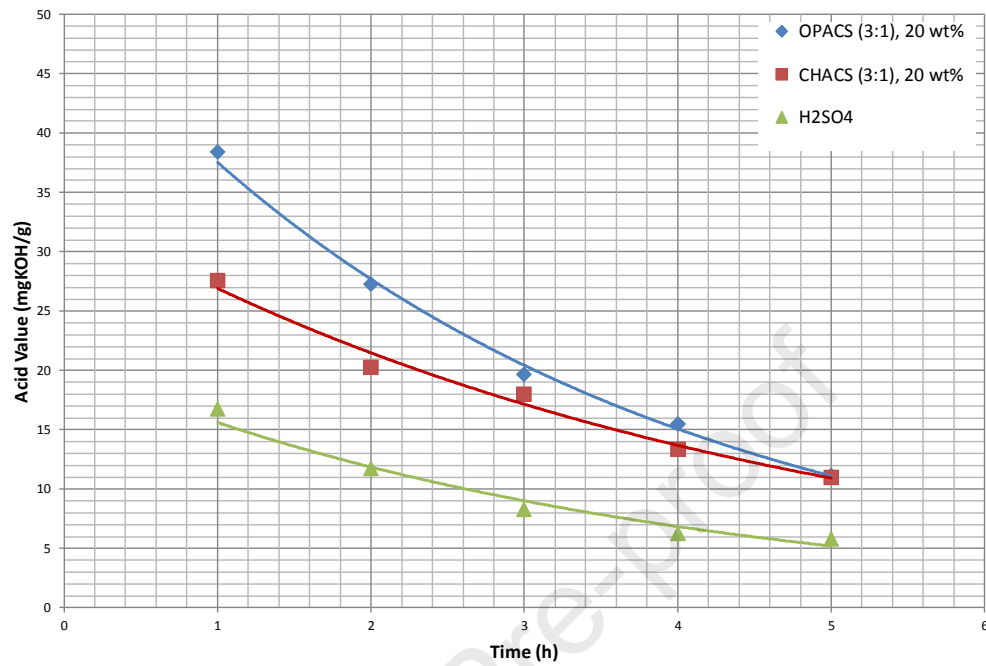


Fig. 6. Acid value evolution of oil using OPACS (sulfonated olive pomace activated carbon), CHACS (sulfonated commercial coconut husk based activated carbon) and Sulfuric acid using 3:1 methanol to FFA molar ratio

## Highlights

- Olive Pomace (OP) is suitable for activated carbon (AC) production
- Sulfonation of olive pomace leads to a good specific surface
- Sulfonated OPAC's structural characteristics allows it to be used as solid catalyst
- Sulfonated AC gives better catalytic performances as compared to  $\text{H}_2\text{SO}_4$
- Hydrophobicity of AC has significant effects on  $\text{SO}_3\text{H}$  fixation and on catalysis

Journal Pre-proof

Declarations of interest: none

Journal Pre-proof